electronics

MDPI

Article

A Novel Portable Solar Powered Wireless Charging Device

Chiang Liang Kok [1,*], Xuanyao Fu [1], Yit Yan Koh [1] and Tee Hui Teo [2]

[1] College of Engineering, Science and Environment, University of Newcastle, Callaghan, NSW 2308, Australia; xuanyao.fu@uon.edu.au (X.F.); yityan.koh@newcastle.edu.au (Y.Y.K.)
[2] Engineering Product Development, Science, Mathematics and Technology, Singapore University of Technology and Design, Singapore 487372, Singapore; tthui@sutd.edu.sg
* Correspondence: chiangliang.kok@newcastle.edu.au

Abstract: This paper presents the development of a portable solar panel wireless charging device with an advanced charging algorithm. The device features a 6500 mAh Li-ion battery and is designed to efficiently charge smartphones and laptops. It incorporates a simulated solar panel, charging circuit, microcontroller, and wireless charging circuits. Rigorous testing has demonstrated its stable output voltage and current at 5 V/2 A, with high power transfer efficiency. The advanced charging algorithm optimizes power transfer efficiency and reduces charging time by adjusting the current and voltage to match the device's needs. This smart approach extends battery life and improves device performance. The device utilizes the Basic MPPT P&O Algorithm to dynamically track the solar panel's Maximum Power Point and optimize power extraction. The Lithium Battery Charging Characteristic Algorithm adjusts the charging levels to ensure safe and efficient charging. However, challenges were encountered during implementation and testing, highlighting the complexities of real-world scenarios and the need for further optimization. The device offers a sustainable and environmentally friendly charging alternative, particularly in areas with limited power access. The research findings contribute to the field of wireless charging, driving advancements in sustainable and efficient technologies.

Keywords: solar energy; wireless charging; MPPT (maximum power point tracking); lithium-ion battery (18,650); PWM (pulse width modulation); circuit design; LTspice; STM32

check for updates

Citation: Kok, C.L.; Fu, X.; Koh, Y.Y.; Teo, T.H. A Novel Portable Solar Powered Wireless Charging Device. *Electronics* **2024**, *13*, 403. https://doi.org/10.3390/electronics13020403

Academic Editor: Alessandro Gabrielli

Received: 13 December 2023
Revised: 9 January 2024
Accepted: 17 January 2024
Published: 18 January 2024

Copyright: © 2024 by the authors. Licensee MDPI, Basel, Switzerland. This article is an open access article distributed under the terms and conditions of the Creative Commons Attribution (CC BY) license (https://creativecommons.org/licenses/by/4.0/).

1. Introduction

A wired cable has a big disadvantage while charging a mobile device since the USB charging connector, which is frequently used, is easily destroyed and shortens the product's lifespan [1]. People today increasingly rely on smart devices to perform tasks when they are out and about. It is crucial to have a portable gadget that can be charged and powered by solar energy because most smart devices are powered by lithium batteries. Lithium is the lightest metal and has the greatest electrochemical potential when compared to other electrochemical metals. This results in a metal with a comparatively high energy density for weight when compared to several other metals. Since lithium metal is highly unstable when charged, there are numerous approaches. Batteries are made using lithium-ion rather than the more common lithium metal. It is safer and simpler to control even if it has a little lower energy density than lithium metal. This not only shortens the lifespan of the devices but also poses a challenge for users who are constantly on the move or in areas with limited access to power sources. This issue can be resolved by using a portable wireless charging system that combines a solar panel to utilize solar energy for off-site charging [2].

This paper will be focused on designing and building a solar-powered Li-ion power bank with a capacity of approximately 6500 mAH and the ability to produce an output of 5 V at 2 A. Wireless charging (magnetic induction) and solar (or DC) input are both possibilities for recharging the battery. The LCD functions as a monitor to check voltage, current, and temperature as well as give feedback to the MCU in the Li-ion battery charger,

which is based on the combination of MPPT and battery charging algorithms utilizing a DC–DC buck converter.

The proposed device offers several relative advantages and benefits compared to existing works. Firstly, it achieves enhanced charging efficiency through the integration of advanced MPPT algorithms and the Li-ion battery charging characteristic algorithm, resulting in optimized power transfer efficiency, reduced charging time, and improved overall charging performance. Secondly, its portability and utilization of solar energy make it well-suited for users on the go and in areas with limited access to power sources. This aspect provides a sustainable and environmentally friendly charging alternative, reducing dependence on traditional charging methods. Lastly, the device incorporates user-friendly features such as an MCU and LCD monitor, which offer real-time feedback on charging parameters, enhancing user control and convenience. Additionally, its compatibility with a wide range of electronic devices further contributes to its user-friendly nature.

The rationale behind the development of the proposed device lies in addressing the limitations of wired cables and the need for sustainable charging solutions for mobile devices. The vulnerabilities of USB charging connectors and the increasing reliance on smart devices necessitate the development of portable wireless charging systems. By harnessing solar energy and incorporating advanced charging algorithms, the device offers a versatile and efficient charging solution.

The MCU acts as the prototype's brain for the primary scope and uses an algorithm to manage the converter's functioning and link the LCD to the display [3]. To offer a proper charging environment for the wireless charging unit, the class AB amplifier will increase the current and the DC–DC boost converter can step up the voltage for the additional scope. The alternative charging function can use the output of the boost converter directly using DC output to charge the mobile device.

Figure 1 below shows the general project block diagram with the main scope and additional scope. Table 1 below contains a collection of design specifications, which include the detailed output power of the solar panel, the battery information, and the wireless charging requirement.

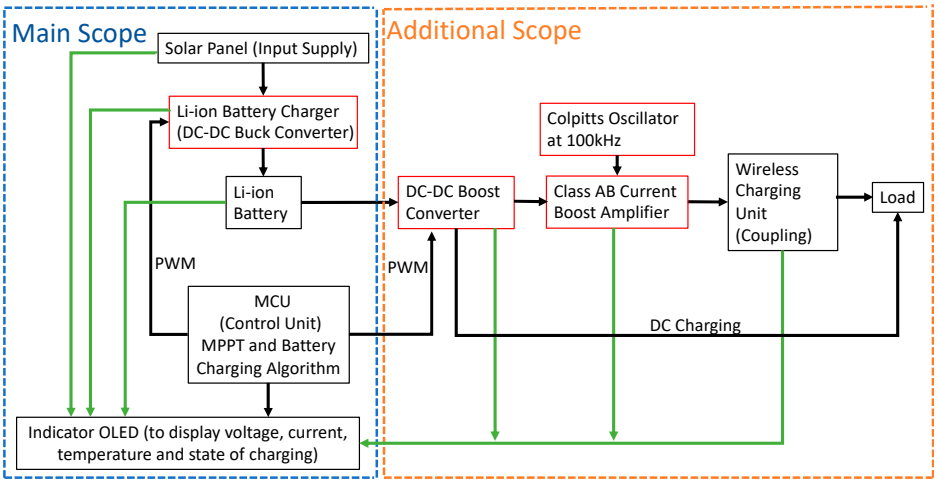


Figure 1. General project block diagram with main scope and additional scope.

Table 1. Design specifications.

Parameters	Values
Solar Panel	20 W (10 V at 2 A)
Battery Voltage	3.7 V Li-ion battery
Charging Battery Voltage	4.2 V
Charging Battery Current	2 A ± 0.2 A
Discharging Battery Current	1 A, Maximum 3 A
Battery Capacity	6500 mAh
Wireless Charging Unit Specification	5 V at 2 A

2. Charging Algorithm Design

2.1. 18,650 Li-ion Battery Charging Algorithm

An example of a rechargeable lithium-ion battery is an 18,650 battery. The battery's size—18 mm diameter and 65 mm length—is indicated by the term 18,650. These batteries are frequently found in portable electrical devices including power banks, computers, and smartphones. They are also utilized in electric cars and other situations that call for a large, rechargeable battery. The advantages of 18,650 batteries include their high energy density, lengthy lifespan, and reasonable price.

Figure 2 below shows the charging characteristics of a lithium-ion battery in three stages.

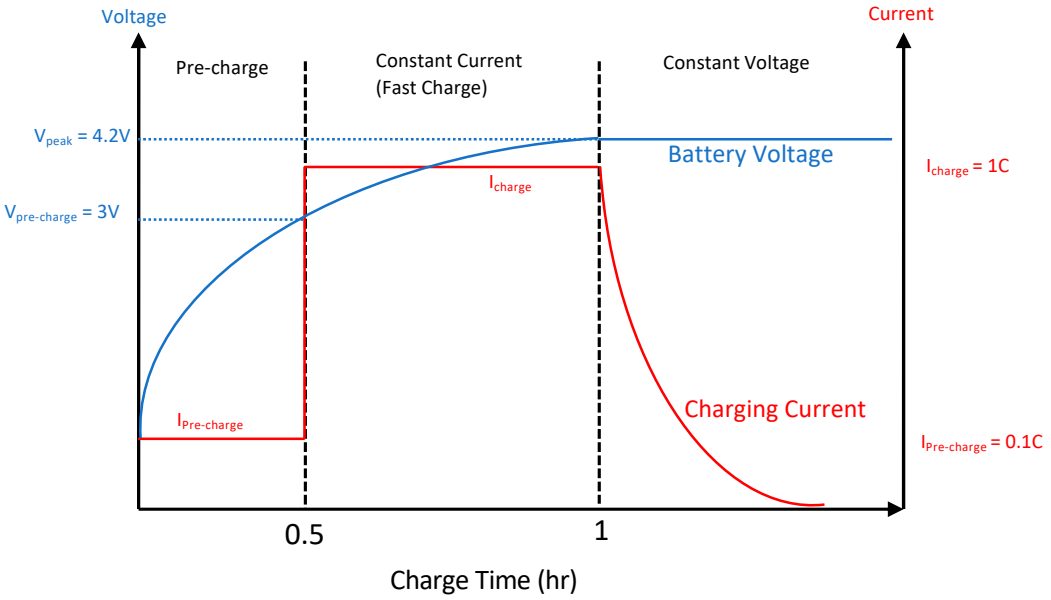


Figure 2. Charging characteristic curve of lithium battery.

Figure 3 below shows the battery charging algorithm flowchart based on the 18,650 Li-ion battery charging feature. This designed algorithm flow chart is improved from the CC/CV charging method in the article "Design and Prototype Modelling of a CC/CV Electric Vehicle Battery Charging Circuit" [4], where SOC is the state of charge, V_{DC} and I_{DC} are the DC charging voltage and current, and I_{min} is the minimum charging current.

This developed portable solar panel wireless charging device features a charging algorithm that consists of three stages: Pre-charge Phase (Trickle Charge/TC), Constant Current Phase (CC), and Constant Voltage Phase (CV) [5]. During the Pre-charge Phase, the voltage is controlled between 2.9 V and 3 V, and the charging current is generally allowed to be below C/10 (150 mA) to slowly charge the battery at a safe and stable level. In the Constant Current Phase, a constant current of 1.6 A is used to charge the battery with a voltage between 3 V and 4.2 V, efficiently charging the battery while ensuring the voltage remains within the manufacturer's recommended limit. Finally, in the Constant Voltage Phase, a constant voltage of 4.2 V is used to charge the battery with a current between 1.6 A and 0 A, which completes the charging process by maintaining a constant voltage while gradually reducing the current.

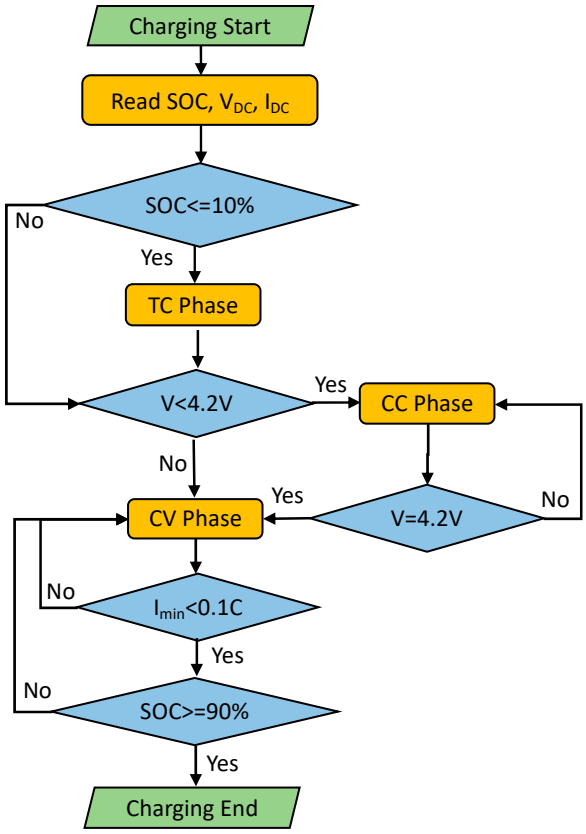


Figure 3. Developed battery charging characteristic algorithm flowchart.

2.2. MPPT (Maximum Power Point Tracking) Algorithm

Figure 4 shows a basic P&O (Perturb and Observe) algorithm flowchart, where ΔD is the duty cycle percentage for the system to adjust; D(t) and D are the current duty cycle at a certain point in time; V, I, and P are the voltage, current, and power; V(t) and P(t) are the present voltage and power the system measured; and V(t − 1) and P(t − 1) are the voltage and power one second before [6].

This flowchart demonstrates how the system measures the voltage and current to calculate the power first, compare the current power to the second power, and then use the voltage to determine if the duty cycle is increasing or decreasing so that the power can be maintained. This algorithm is improved from the flowchart of the modified P&O MPPT algorithm in the article "A modified P&O MPPT algorithm for single-phase PV systems based on deadbeat control" [7] and the MPPT P&O algorithm flowchart in the article "Change in Power based P&O Algorithm for Maximum Power Extraction in Solar Energy Conversion System" [8].

In the Basic P&O (Perturb and Observe) algorithm flowchart for MPPT (Maximum Power Point Tracking), the variables D, ΔD, D(t), and D represent the duty cycle of the system. The duty cycle is a control parameter that determines the ON and OFF periods of the power converter in the MPPT system. To clarify, the equations D = D − ΔD and D = D + ΔD in the algorithm do not directly correspond to current and voltage. Instead, they represent the adjustment of the duty cycle based on the measured voltage and power values. In the P&O algorithm, the duty cycle is adjusted based on the change in power (P) relative to the previous measurement (P(t − 1)). This algorithm aims to track the maximum power point (MPP) by iteratively adjusting the duty cycle and observing the effect on the power output. To differentiate between current (I) and voltage (V), voltage and current sensors were used to measure both parameters. These measurements can also be used in conjunction with the P&O algorithm to track the MPP accurately.

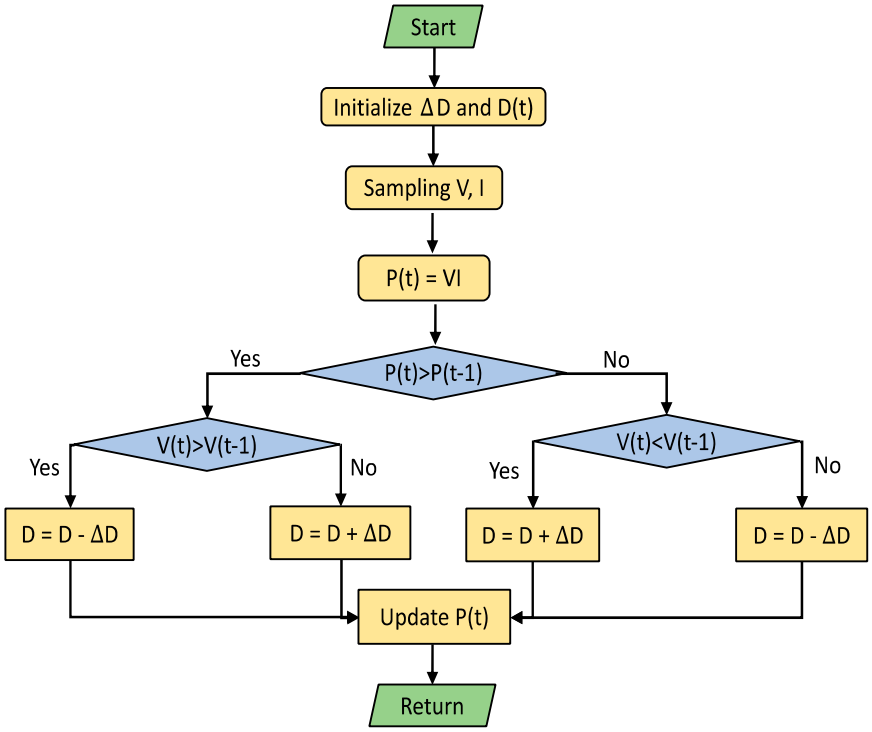


Figure 4. Developed basic P&O algorithm flowchart.

2.3. Merged MPPT and 18,650 Battery Charging Algorithm

Based on the previous MPPT algorithm and Li-ion battery charging algorithm discussed in Figures 3 and 4, the two algorithms merge to create a new charging algorithm shown in Figure 5. This algorithm is improved from the flowchart of the modified constant voltage MPPT algorithm in the article "The Fastest MPPT Tracking Algorithm for a PV array fed BLDC Motor Driven Air Conditioning system" [9] and the algorithm of the proposed MPPT technique figure in the article "Design of a charge controller based on SEPIC and buck topology using modified Incremental Conductance MPPT" [10].

Merging MPPT and Li-ion battery charging algorithms in a constant current phase together can be achieved by implementing a control algorithm that takes into account the input voltage and current of the solar panel, the battery voltage and current, and the desired charging parameters of the Li-ion battery.

During the Pre-charge Phase, the voltage is controlled between 2.9 V and 3 V, and the charging current is generally allowed to be below C/10 (150 mA) to slowly charge the battery at a safe and stable level. In the Constant Current Phase, PWM is used to control the duty cycle and input power [11], and a constant current of 1.6 A is used to charge the battery with a voltage between 3 V and 4.2 V. Finally, in the Constant Voltage Phase, a constant voltage of 4.2 V is used to charge the battery with a current between 1.6 A and 0 A, completing the charging process.

The charging algorithm is designed to optimize the power transfer efficiency and reduce the charging time. The device has been tested to a provide stable and reliable output voltage and current of 5 V/2 A while maintaining high power transfer efficiency. The device can offer a sustainable and environmentally friendly alternative to traditional charging methods for electronic devices, particularly in areas with limited access to power sources.

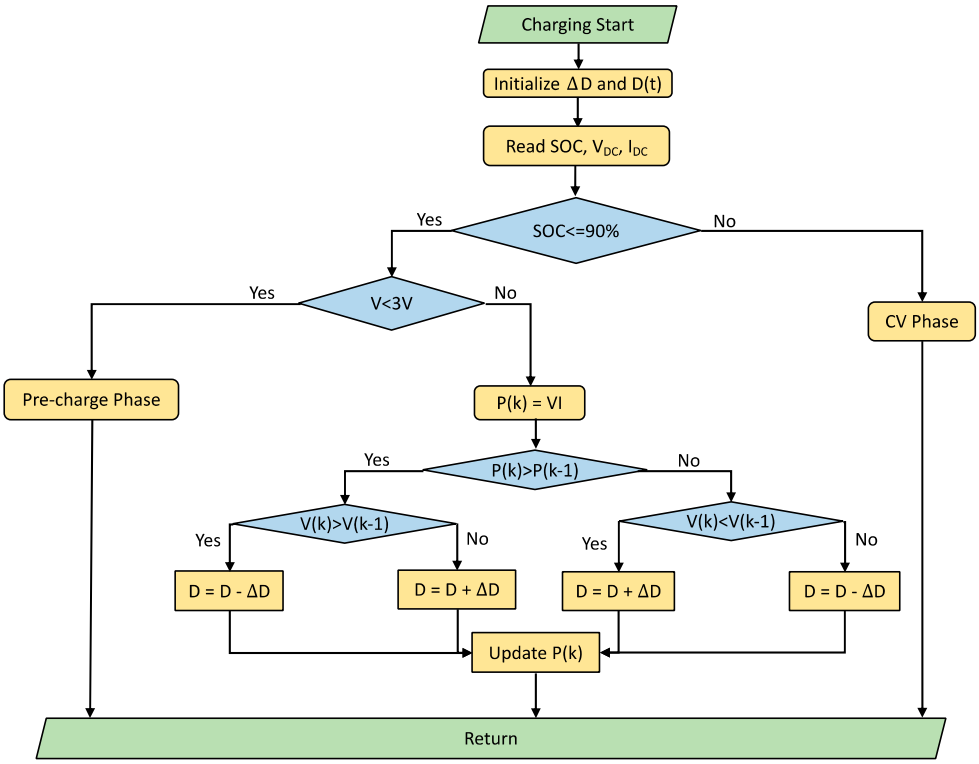


Figure 5. Merged charging algorithm flowchart.

3. Relevant Circuits Design

3.1. Buck Converter Circuit

A DC–DC converter is a type of switched-mode power supply (SMPS) that has at least two semiconductors—a diode and a transistor—and at least one energy storage device, such as a capacitor, an inductor, or both. Boost converters and buck converters are the two basic categories under which DC–DC converters fall. In contrast to buck converters, which reduce input voltage to produce a lower output voltage, boost converters raise input voltage to produce a greater output voltage.

A DC-to-DC converter known as a buck converter lowers the voltage of a DC input signal. To step down the voltage, a transformer is used to transform the input voltage into a high-frequency AC signal. To provide a DC output voltage lower than the input voltage, the AC signal is then rectified and filtered. Three things make up the buck converter: an inductor, a switch, and a diode. When the switch is closed, the inductor stores energy in the form of a magnetic field and releases it when the switch is opened. The diode limits the direction in which current can flow and prevents the inductor from returning the stored energy into the circuit. The switch is cycled on and off at a high frequency, and its duty cycle is adjusted to regulate the buck converter's output voltage. This alters how long the inductor is charged and discharged for, ultimately regulating how much energy is sent to the output. The output voltage of the buck converter can be accurately regulated by modifying the duty cycle.

The buck converter in this project is a DC-to-DC power converter that either steps up current or steps down voltage (10 V to 4.2 V). At heavy loads, synchronous buck converter topology is more efficient [12]. Designing a synchronous buck converter uses Equations (1)–(4) [13], where D is the duty cycle, V_o and V_{in} are the output and input voltage, f_S is the switching frequency, ΔI_L is the assumed load current ripple, L is the inductor value, C is the capacitor value, and C_{in} is the input capacitance. ΔV_L is the assumed output voltage ripple, and ΔV_i is the assumed input voltage ripple.

$$V_o = DV_i \tag{1}$$

$$L = \frac{V_o(1-D)}{f_s(\Delta I_L)} \tag{2}$$

$$C = \frac{\Delta I_L}{8 f_s(\Delta V_o)} \tag{3}$$

$$C_{in} = \frac{I_{in} * (1-D)}{8 f(\Delta V_i)} \tag{4}$$

Figure 6 below shows the designed synchronous N-MOSFET buck converter circuit using IRF540 MOSFET and IR2301S gate driver.

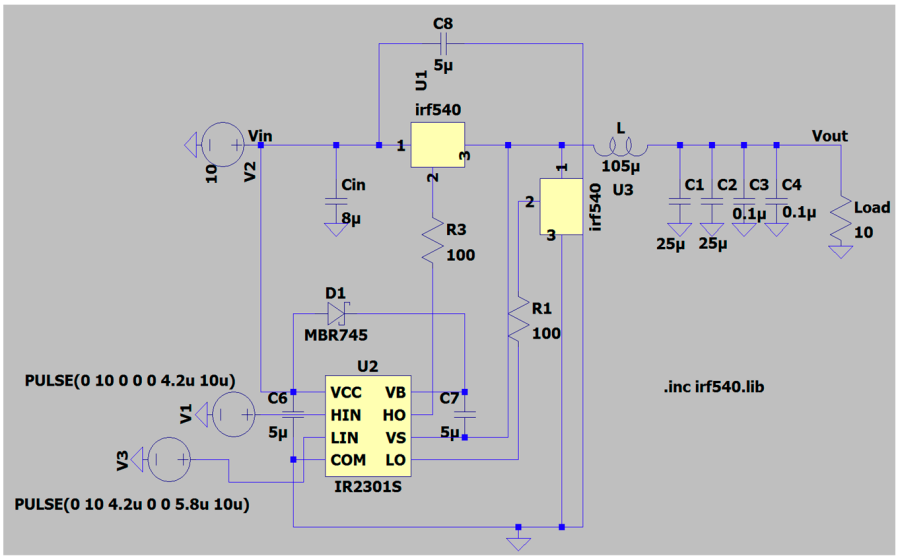


Figure 6. Synchronous N-MOSFET Buck Converter circuit using IRF540 MOSFET and IR2301S Gate Driver on LTspice.

The reason why IRF540N is chosen as the MOSFET for this project is because this MOSFET offers several advantages. It has a high current capability of up to 33 A, making it suitable for high-current applications such as power supplies and motor control. Additionally, it has a low on-resistance of 0.077 ohms, allowing it to switch high currents with minimal power loss and heat dissipation. The IRF540 also has a fast-switching speed of 100 ns, making it suitable for high-frequency applications such as switching power supplies. Its high voltage capability of up to 100 V also allows high-voltage applications such as inverter circuits and DC–DC converters. Finally, the IRF540 is widely available and relatively affordable compared to other high-power MOSFETs, making it a popular and cost-effective choice for many power electronics applications.

An external gate resistor is a resistor that is linked in series with the MOSFET's gate terminal. The primary purposes of the gate resistor are to prevent electrostatic discharge (ESD) and overcurrent damage to the MOSFET by controlling the amount of current flowing into the gate and reducing output ringing. The switching rate of a MOSFET is slowed by a high gate resistance. As a result, power loss increases, and potential heat issues arise. A tiny gate resistor, on the other hand, speeds up a MOSFET's switching rate, making it more susceptible to voltage spikes and oscillations, and, as a result, to failure and device damage.

By doing this, high-frequency oscillations that could be caused by the MOSFET's parasitic capacitances and those of other circuit components are avoided. The MOSFET must be fully turned on for the gate voltage to reach the threshold value fast after the MOSFET comes on. Unfortunately, the sudden increase in gate voltage can result in significant current spikes that might induce ringing and Electromagnetic Interference (EMI) in the circuit.

To guarantee that the MOSFET performs correctly and dependably, it is crucial to select the proper value for the external gate resistor. For the external gate resistor, a value between 1 and 10 kiloohms is typically employed.

The IR2301 was chosen as the gate driver of this project, and it has two independent high- and low-side output channels that provide high peak output current and voltage swing, enabling it to drive high-power devices with fast switching speeds. The IR2301 also has an integrated shutdown function that allows for the easy implementation of over-current and short-circuit protection to improve system reliability. Its wide input voltage range and under-voltage lockout protection make it suitable for a wide range of applications, while its low power consumption helps to reduce system power consumption and improve energy efficiency.

As seen in the diagram, the two PWM signals that control the high-side and low-side MOSFETs should have complementary duty cycles, ensuring that the high-side and low-side MOSFETs do not turn on at the same time, which otherwise could cause a short circuit and damage the circuit. This is because the high-side MOSFET is typically driven by a gate voltage higher than the input voltage, while the low-side MOSFET is driven by a gate voltage lower than the input voltage. If both MOSFETs turn on at the same time, the voltage across them will be very low, and a large current will flow through the circuit, potentially causing damage.

To prevent this, the controller IC generates two complementary PWM signals, ensuring when one MOSFET is on, the other MOSFET is off. For example, if the duty cycle of the PWM signal that drives the high-side MOSFET is 70%, then the duty cycle of the PWM signal that drives the low-side MOSFET should be 30% to ensure that the total duty cycle of the two signals is 100%. This guarantees that both MOSFETs turn on and off at the appropriate times to achieve the desired output voltage, without the risk of a short circuit.

3.2. Boost Converter Circuit

A boost converter is a DC-to-DC power converter that steps up voltage (3.9 V to 5 V) or steps down current. Equations (5)–(7) are used to design a boost converter [14], where D is the duty cycle, V_o and V_{in} are the output and input voltage, I_{out} is the output current, f_S is the switching frequency, ΔI_L is the assumed load current ripple, L is the inductor value, C is the capacitor value, and C_{in} is the input capacitance. ΔV_L is the assumed output voltage ripple.

$$D = 1 - \frac{V_{in}}{V_{out}} \tag{5}$$

$$L = \frac{DV_{in}}{f_s(\Delta I_L)} \tag{6}$$

$$C = \frac{DI_{out}}{f_s(\Delta V)} \tag{7}$$

Figure 7 shows the designed N-MOSFET boost converter circuit using IRF540 MOSFET.

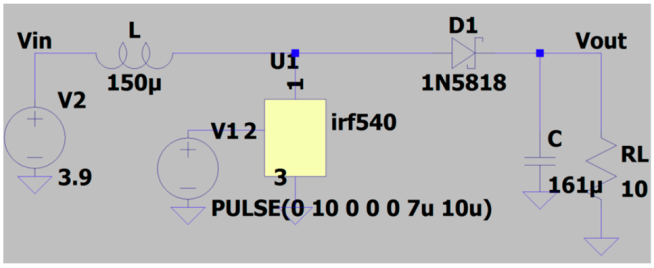


Figure 7. N-MOSFET Boost Converter circuit using IRF540 MOSFET on LTspice.

3.3. Class AB Amplifier Circuit

A class AB power amplifier is used to amplify the current to a higher value so that it may be used for a wireless charging unit, since the battery can only provide a tiny value of DC current for the project to use. The design and simulation of the class AB amplifier utilized in this project will be covered in this part.

The designed Class AB amplifier circuit which follows the design specifications is shown in Figure 8 [15].

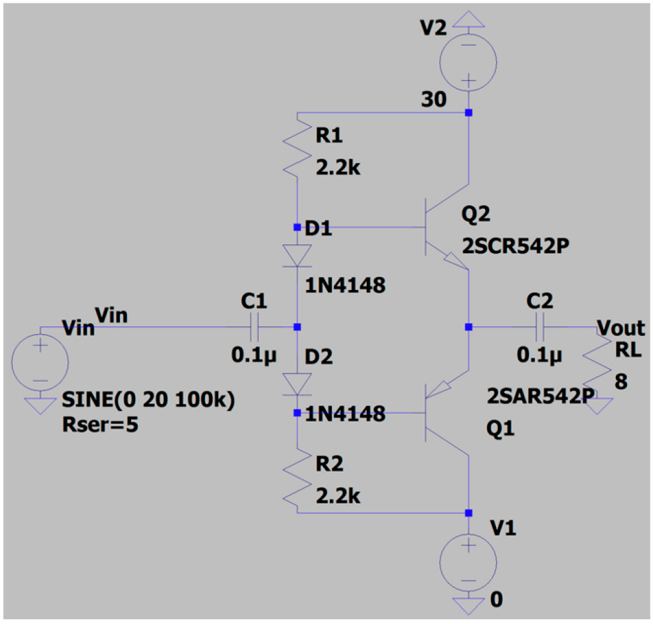


Figure 8. Diodes biasing Class AB amplifier circuit on LTspice.

If the biasing resistor value is small, the diode voltage will be higher, the transistor voltage will be higher, and at this moment the efficiency of this Class AB amplifier will drop. If the biasing resistor value is large, the diode voltage will be too small, so the Class AB amplifier is turned off, and there will be crossover distortion shown in the output signal.

3.4. Colpitts Oscillator Circuit

The battery can only output a DC for the project to use, so a Colpitts oscillator is used to oscillate the voltage at a stable frequency to generate an AC waveform for the wireless charging unit to use. This section will discuss the design and simulation for the Colpitts oscillator used in the project.

Equations (8)–(10) are used to design the Colpitts oscillator, where f_r is the oscillating frequency, L is the inductor value, C_T is the total capacitor value, and C_1 and C_2 are the two capacitor's values in the tank circuit of the oscillator circuit [16].

$$\text{Oscillate frequency} : f_r = \frac{1}{2\pi\sqrt{LC_T}} \tag{8}$$

$$\text{Total capacitance} : C_T = \frac{C_1 * C_2}{C_1 + C_2} \tag{9}$$

$$\text{Feedback fraction} : F_F = \frac{C_1}{C_2} \tag{10}$$

Figure 9 shows the Colpitts oscillator circuit on LTspice [17].

The biasing current of a Colpitts oscillator refers to the amount of current that flows through the biasing resistors that are used to bias the transistor in the oscillator circuit. The biasing current is an important parameter in oscillator design, as it affects the stability, frequency, and output power of the oscillator.

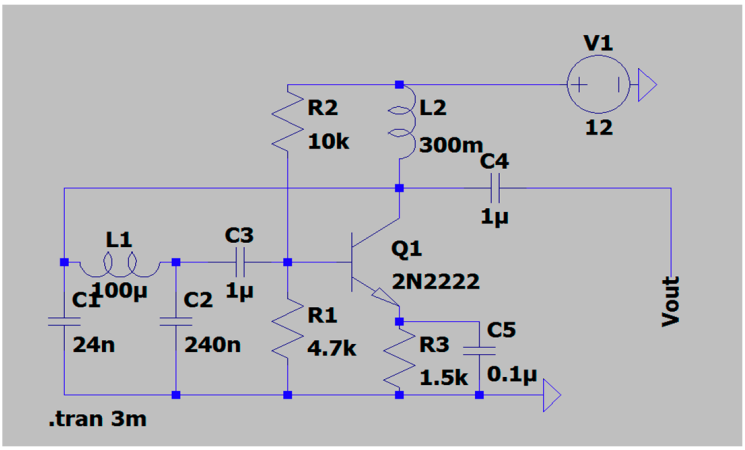


Figure 9. Designed Colpitts oscillator circuit on LTspice.

To improve the biasing current in a Colpitts oscillator, one can choose appropriate biasing resistors, and the value of the biasing resistors should be chosen so that they provide the correct amount of biasing current for the transistor used in the oscillator circuit. A higher-value resistor can increase the biasing current, but it can also reduce the output power and lower the frequency of oscillation.

4. Implementation

4.1. Laboratory Test Circuit Output Result

Figures 10–13 show the Colpitts oscillator and Class AB amplifier breadboard circuit simulation and laboratory test and voltage output results when the input voltage supply to the oscillator is a DC at 15 V.

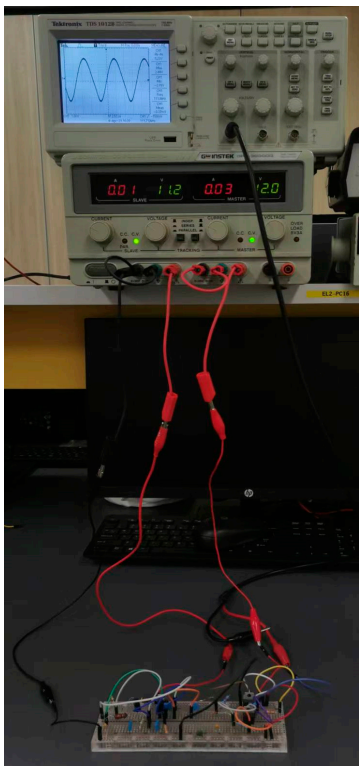


Figure 10. Breadboard prototype of Colpitts Oscillator and Class AB amplifier laboratory test.

When the input voltage of this oscillator and the Class AB amplifier combined circuit is at 11.2 V DC, the simulation result will output a stable and clear peak-to-peak voltage of

around 12 V. For the breadboard testing, the peak-to-peak voltage drops to around 5.2 V due to the EMI and other effects, but it still has a frequency of around 100 kHz. As a result, this output voltage is the generated final signal to charge the wireless charging unit.

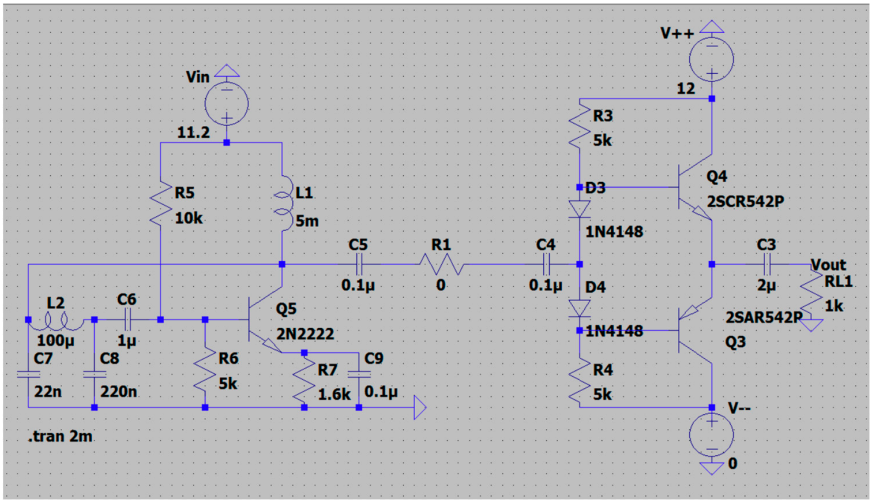


Figure 11. Equivalent circuit of Colpitts oscillator and Class AB amplifier laboratory test.

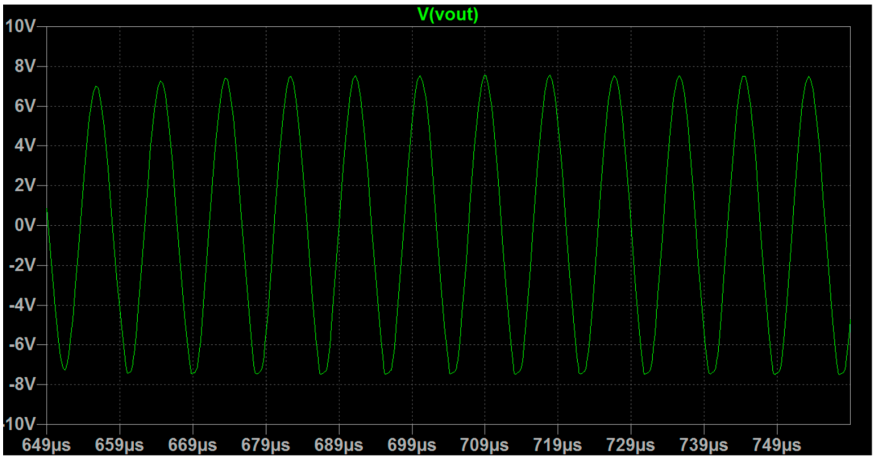


Figure 12. Colpitts oscillator and Class AB amplifier laboratory test equivalent circuit simulation result.

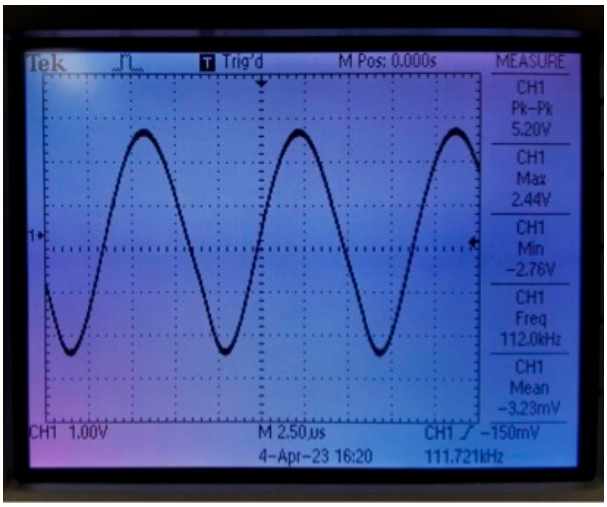


Figure 13. Colpitts oscillator and Class AB amplifier prototype laboratory voltage output oscilloscope result.

4.2. Overall Prototype Output Result

Using a DC power supply to replace the solar panel, the relevant circuits and batteries were assembled into a prototype of the device using an STM32 microcontroller. Figure 14 shows the overall built project board prototype using wireless charging to charge a mobile phone.

After all the circuits are connected, this prototype can realize the wireless charging function and make the mobile phone charge stably with an inductive coupling [18] wireless charging unit. The time taken to fully charge a mobile phone with a 2800 mAh capacity battery is around 3 h via DC wired charging and 4 h via wireless charging. Figure 15 shows the charging state of these two charging methods.

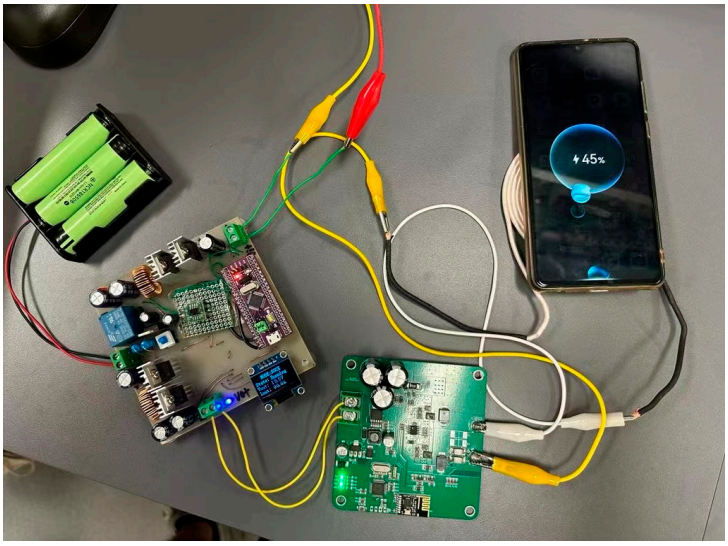


Figure 14. Designed project prototype output wireless charging mobile phone.



Figure 15. Time vs. charging state (percentage) with wired and wireless charging methods.

4.3. Improved Buck/Boost Converter Circuit Using PCB Board

Figure 16 shows the designed synchronous buck converter PCB diagram.

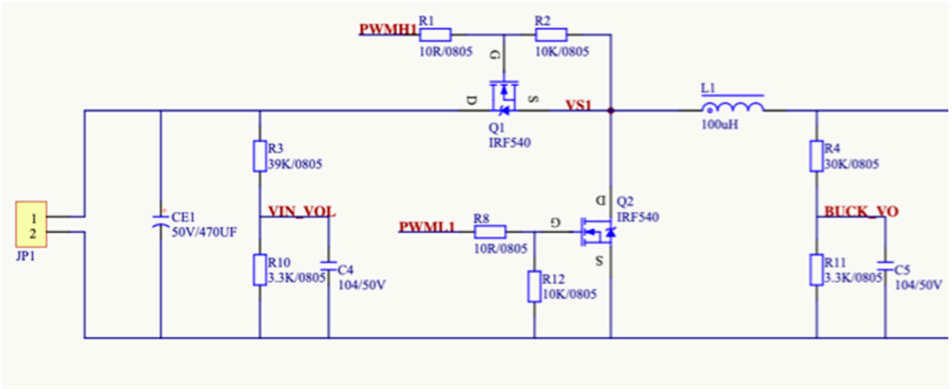


Figure 16. Synchronous buck converter PCB diagram.

The basic operation of a buck converter involves switching a series-connected inductor and a switch (usually a MOSFET) on and off at a high frequency. This generates a square-wave voltage waveform across the inductor, which causes the inductor to store and release energy to the output capacitor and load.

A relay circuit on the right is used to disconnect the load from the buck converter in case of a fault or overload condition. This prevents damage to the load and the converter and can improve safety. The relay can be controlled by a sensing circuit that detects the load current or voltage and triggers the relay if it exceeds a certain threshold. It is also used to protect the buck converter and the battery from overvoltage or reverse polarity at the output of the buck converter. This relay can be controlled by a protection circuit that monitors the input voltage and triggers the relay if it exceeds a certain level or polarity.

Figure 17 shows the designed boost converter PCB diagram.

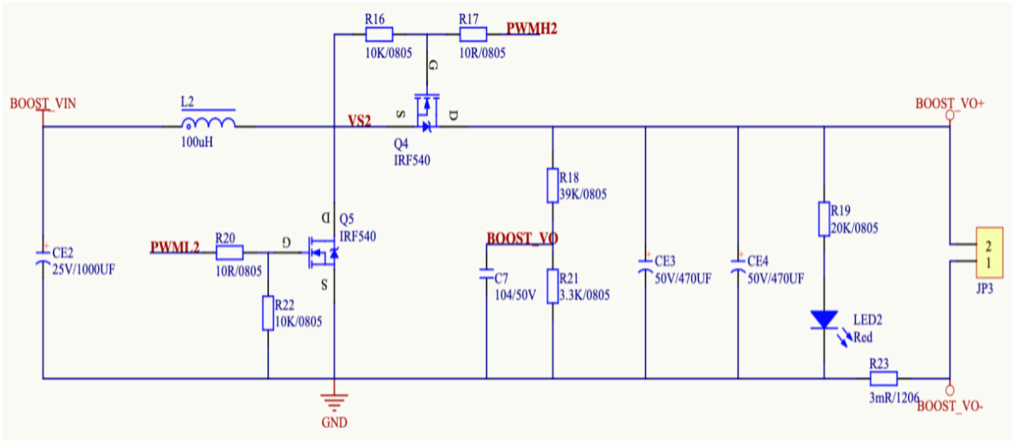


Figure 17. Boost converter PCB diagram.

This synchronous boost converter is a type of DC–DC converter that can step up a lower voltage to a higher voltage. The basic operation of a synchronous boost converter involves switching two series-connected switches (usually MOSFETs) on and off at a high frequency. This generates a square-wave voltage waveform across an inductor and a capacitor, which causes the inductor to store and release energy to the output capacitor and load.

The design specification for a synchronous boost converter will depend on the specific application requirements, such as the input and output voltage range, the maximum output current, the efficiency, and the size and cost constraints. Some key design parameters include the inductor value, the switching frequency, the duty cycle, the MOSFET specifications, and the output capacitor value. The proper selection and optimization of these

parameters can help to achieve high efficiency, low output ripple, and reliable operation of the synchronous boost converter.

Figure 18 shows the improved buck/boost converter circuit implemented using a double-layer PCB board which was designed using Altium Designer software and fabricated by JLCPCB (Version 24.0.1). It measured 13 cm by 12 cm.

The size and shape of the PCB board will depend on the size of the components and the space available in the project enclosure.

Making sure that the high-current wiring stays far enough away from the low-current wiring is one of the most important things to do to increase the stability of the system, since this could lead to several stability problems. Most of the battery's high-current wire is located at the top layer and is identified by the colour red. The wiring is being segregated to ensure that the other electrical components, especially the voltage sensors, will not be harmed because the battery will always change in voltage and have high current changes. To make sure that the circuit wiring can take high current during the battery's charge and discharge, the wiring is also thicker on the side with a greater current.

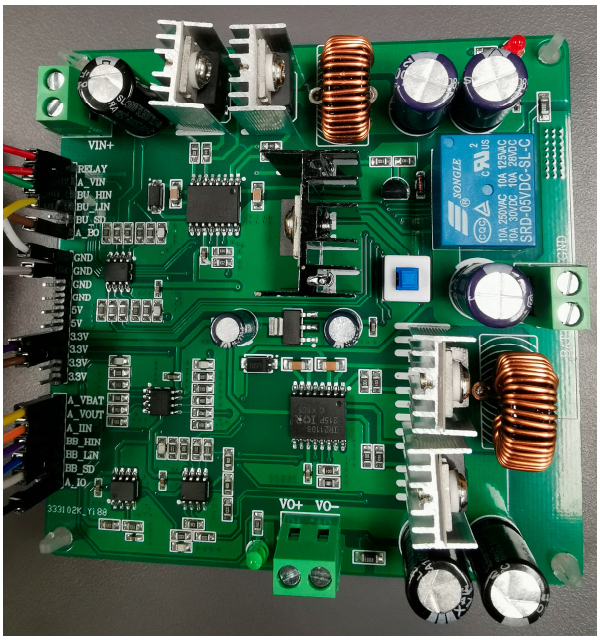


Figure 18. Buck/boost converter PCB prototype.

To decrease reading fluctuation and improve voltage sensing accuracy, the wiring for the voltage sensor must be as close as feasible to the pin it will measure and to the MCU ADC port. Additionally, the wiring for the sensors is laid out so that it is not near any other wires that might interfere with the detection, which can attach red wires to the PCB's underside. The PWM signals used to control cell balancing are routed along those lines. The PWM wiring from the MCU is jumped across the sensing path to the top layer to ensure that it will not interfere with it. To make it simpler to attach the top wiring to the component legs of the cell balancing circuits, it is then connected back to the bottom layer.

Routing is the process of connecting the components and traces on the PCB board, using the auto-routing function or manual routing tools to optimize the routing and minimize trace length and interference. Also, ground planes or power planes are used to reduce the noise and improve signal integrity. The layer stack-up refers to the number and arrangement of the layers in the PCB board. The layer stack-up can affect the signal integrity, the EMI/EMC performance, and the cost of the PCB board.

5. Conclusions

In conclusion, this research presents a significant advancement in the development of portable charging solutions. The proposed solar-powered Li-ion power bank, with its advanced charging algorithm and wireless charging capabilities, addresses the challenges associated with the frequent use and potential damage of USB charging connectors. By harnessing solar energy, it provides a sustainable and environmentally friendly alternative to traditional charging methods, particularly beneficial for users in areas with limited access to power sources. The incorporation of open-loop and closed-loop MPPT methods, along with real-time monitoring of output voltage and current, ensures optimal power extraction and efficient charging. Despite the complexities encountered during implementation and testing, the findings contribute to the broader field of wireless charging devices and pave the way for further advancements in sustainable and efficient charging technologies. Future work will focus on refining the algorithms and enhancing the device's performance in real-world scenarios.

Author Contributions: Conceptualization, Resources and Software, C.L.K.; Methodology, Data Curation and Investigation, X.F.; Methodology, Visualization and Formal Analysis, Y.Y.K.; Supervision and Funding Acquisition, T.H.T. All authors have read and agreed to the published version of the manuscript.

Funding: This research received no external funding.

Data Availability Statement: The data presented in this study are available in this article.

Acknowledgments: The authors would like to extend their appreciation to the University of Newcastle, Australia, for financing the project possible.

Conflicts of Interest: The authors declare no conflicts of interest.

References

1. Bari, M.F.; Chowdhury, M.R.; Sen, S. Is Broken Cable Breaking Your Security? In Proceedings of the 2023 IEEE International Symposium on Circuits and Systems (ISCAS), Monterey, CA, USA, 21–25 May 2023; pp. 1–5.
2. Muhseen, Z.; Sundar, V.; Balakrishnan, M.; Ravi, V.; Prathibha, S.; Ganesh, D.; Sathiyanarayanan, M. Portable Smart Solar Panel for Consumer Electronics. In Proceedings of the 2020 International Conference on Smart Technologies in Computing, Electrical and Electronics (ICSTCEE), Bengaluru, India, 9–10 October 2020; pp. 494–499.
3. Sutar, A.V.; Dighe, V.; Karavkar, P.; Mhatre, P.; Tandel, V. Solar Energy based Mobile Charger Using Inductive Coupling Transmission. In Proceedings of the 2020 4th International Conference on Intelligent Computing and Control Systems (ICICCS), Madurai, India, 13–15 May 2020; pp. 995–1000.
4. Thomson, S.J.; Thomas, P.; Anjali, R.; Rajan, E. Design and Prototype Modelling of a CC/CV Electric Vehicle Battery Charging Circuit. In Proceedings of the 2018 International Conference on Circuits and Systems in Digital Enterprise Technology (ICCSDET), Kottayam, India, 21–22 December 2018; pp. 1–5.
5. Weixiang, S.; Thanh Tu, V.; Kapoor, A. Charging algorithms of lithium-ion batteries: An overview. In Proceedings of the 2012 7th IEEE Conference on Industrial Electronics and Applications (ICIEA), Singapore, 18–20 July 2012; pp. 1567–1572.
6. Alrubaie, A.J.; Al-Khaykan, A.; Malik, R.Q.; Talib, S.H.; Mousa, M.I.; Kadhim, A.M. Review on MPPT Techniques in Solar System. In Proceedings of the 2022 8th International Engineering Conference on Sustainable Technology and Development (IEC), Erbil, Iraq, 23–24 February 2022; pp. 123–128.
7. Yang, Y.; Blaabjerg, F. A modified P&O MPPT algorithm for single-phase PV systems based on deadbeat control. In Proceedings of the 6th IET International Conference on Power Electronics, Machines and Drives (PEMD 2012), Bristol, UK, 27–29 March 2012; pp. 1–5.
8. Madhu, G.M.; Vyjayanthi, C.; Modi, C. Change in Power based P&O Algorithm for Maximum Power Extraction in Solar Energy Conversion System. In Proceedings of the 2021 9th IEEE International Conference on Power Systems (ICPS), Kharagpur, India, 16–18 December 2021; pp. 1–6.
9. Munisekhar, S.; Marutheswar, G.V.; Sujatha, P. The Fastest MPPT Tracking Algorithm for a PV array fed BLDC Motor Driven Air Conditioning system. In Proceedings of the 2019 5th International Conference on Electrical Energy Systems (ICEES), Chennai, India, 21–22 February 2019; pp. 1–5.
10. Latif, T.; Hussain, S.R. Design of a charge controller based on SEPIC and buck topology using modified Incremental Conductance MPPT. In Proceedings of the 8th International Conference on Electrical and Computer Engineering, Dhaka, Bangladesh, 20–22 December 2014; pp. 824–827.
11. Takimoto, T.; Kuchii, S. Control of DC-DC converters with pulse width modulation inputs. In Proceedings of the 2009 ICCAS-SICE, Fukuoka, Japa, 18–21 August 2009; pp. 896–898.

12. Eraydin, H.; Bakan, A.F. Efficiency Comparison of Asynchronous and Synchronous Buck Converter. In Proceedings of the 2020 6th International Conference on Electric Power and Energy Conversion Systems (EPECS), Istanbul, Turkey, 5–7 October 2020; pp. 30–33.
13. Palanidoss, S.; Vishnu, T.V.S. Experimental analysis of conventional buck and boost converter with integrated dual output converter. In Proceedings of the 2017 International Conference on Electrical, Electronics, Communication, Computer, and Optimization Techniques (ICEECCOT), Mysuru, India, 15–16 December 2017; pp. 323–329.
14. Visalakshi, S.; Raj, R.I.; Aswin, M.; Santhosh, R.; Yuwaraj, A. Performance Improvement of Solar Cell using Modified Boost Converter. In Proceedings of the 2023 4th International Conference on Signal Processing and Communication (ICSPC), Coimbatore, India, 23–24 March 2023; pp. 412–416.
15. Shukla, S.; Pandey, B.; Srivastava, S. New circuit models of Complementary-Symmetry Class-AB and Class-B Push-Pull Amplifiers. In Proceedings of the 2012 10th IEEE International Conference on Semiconductor Electronics (ICSE), Kuala Lumpur, Malaysia, 19–21 September 2012; pp. 538–542.
16. Imani, A.; Hashemi, H. Frequency and Power Scaling in mm-Wave Colpitts Oscillators. *IEEE J. Solid-State Circuits* **2018**, *53*, 1338–1347. [CrossRef]
17. Chung, C.; Chao, S. Robust Colpitts and Hartley oscillator design. In Proceedings of the 2014 IEEE International Frequency Control Symposium (FCS), Tampa, FL, USA, 19–22 May 2014; pp. 1–6.
18. Lu, X.; Wang, P.; Niyato, D.; Kim, D.I.; Han, Z. Wireless Charging Technologies: Fundamentals, Standards, and Network Applications. *IEEE Commun. Surv. Tutor.* **2016**, *18*, 1413–1452. [CrossRef]

Disclaimer/Publisher's Note: The statements, opinions and data contained in all publications are solely those of the individual author(s) and contributor(s) and not of MDPI and/or the editor(s). MDPI and/or the editor(s) disclaim responsibility for any injury to people or property resulting from any ideas, methods, instructions or products referred to in the content.